frontiers | Frontiers in Marine Science

TYPE Original Research
PUBLISHED 06 October 2022
DOI 10.3389/fmars.2022.976543



OPEN ACCESS

EDITED BY
Fei Chai,
Ministry of Natural Resources, China

REVIEWED BY
Satya P. Singh,
Saurashtra University, India
Jochen Schmid,
University of Münster, Germany

*CORRESPONDENCE
Mutai Bao
mtbao@ouc.edu.cn

SPECIALTY SECTION
This article was submitted to Marine Biogeochemistry, a section of the journal Frontiers in Marine Science

RECEIVED 23 June 2022
ACCEPTED 22 September 2022
PUBLISHED 06 October 2022

CITATION
Hu X, Li F, Zhang X, Pan Y, Lu J, Li Y and Bao M (2022) The structure, characterization and dual-activity of exopolysaccharide produced by *Bacillus enclensis* AP-4 from deep-sea sediments.
*Front. Mar. Sci.* 9:976543.
doi: 10.3389/fmars.2022.976543



# The structure, characterization and dual-activity of exopolysaccharide produced by *Bacillus enclensis* AP-4 from deep-sea sediments

Xin Hu[1,2], Fengshu Li[1,2], Xiuli Zhang[3], Yaping Pan[1,2], Jinren Lu[1,2], Yiming Li[1,2] and Mutai Bao[1,2]*

[1]Frontiers Science Center for Deep Ocean Multispheres and Earth System, Key Laboratory of Marine Chemistry Theory and Technology, Ministry of Education, Ocean University of China, Qingdao, China, [2]College of Chemistry & Chemical Engineering, Ocean University of China, Qingdao, China, [3]Key Laboratory of Marine Drugs, Ministry of Education, School of Medicine and Pharmacy, Ocean University of China, Qingdao, China

In recent years, the exopolysaccharide (EPS) produced by deep-sea bacteria has attracted the interest of various researchers. In the present study, we have explored the properties and structure of a novel exopolysaccharide (called BPS) produced by *Bacillus enclensis* AP-4 from deep-sea sediments. The maximum yield of BPS was 4.23 ± 0.17 g $L^{-1}$ in a 2216E modified medium. $^{1}$H NMR studies of the purified BPS displayed α and β-configuration sugar residues, including mannose, glucosamine, glucose, galactose, and xylose in a molar ratio of 1.00: 0.09: 0.04: 0.09: 0.07. BPS showed a molecular weight of 23,434 Da and was abundant in hydroxyl and amino residues. In addition, BPS exhibited a rod-like structure with a rough surface and was dominated by C, N, and O elements. The exopolysaccharide demonstrated remarkable thermal stability, high degradation temperature, and excellent emulsification capacity compared to most reported exopolysaccharides. Moreover, BPS displayed better quenching activities against the four radicals, which provided favorable protection for the strain. Finally, the freezing experiment investigated the cryoprotective effect of BPS on *E. coli* and *S. aureus*. BPS effectively improved the cell survival ratio and maintained the activity of $Na^{+}/K^{+}$-ATPase, which facilitates culture preservation. To the best of our knowledge, our work is the first report suggesting that marine exopolysaccharide has dual-activity. This work presents the foundation for the analysis of the structure and properties of exopolysaccharides produced by deep-sea bacteria.

KEYWORDS

**exopolysaccharide, Bacillus sp., deep-sea bacteria, antioxidant activity, cryoprotective activity**

# Introduction

Microbial resources are abundant in nature and rich in beneficial biological properties. Microbes can survive in diverse environments such as high salinity, high pressure, and low temperature since they strengthen themselves through molecules or mechanisms (Andrew and Jayaraman, 2020). The defense mechanisms that lead to microbial adaptability are achieved through various metabolites such as enzymes, peptides, and polysaccharides (Poli et al., 2017). Furthermore, microbial polysaccharides are classified into exopolysaccharides (EPSs), intracellular polysaccharides, and cell wall polysaccharides. EPSs have received extensive consideration owing to their excellent oxidation resistance, emulsification properties, and protection ability in recent years (Jing et al., 2017; Feng et al., 2021; Chen et al., 2022).

EPS-producing bacteria are widely distributed in marine ecosystems and can be isolated from water, sediments, and animals (Costaouëc et al., 2012). EPSs produced by marine bacteria usually have multiple physiological roles involved in the responses to environmental stress, intercellular interactions, and in adherence to surface substances (Wang et al., 2019). The relative significance of these functions often depends on the environment in which bacteria survive. Moreover, marine EPSs can capture nutrients, maintain enzyme activities and provide protection against other toxic substances (Satpute et al., 2010). Furthermore, several factors such as chemical composition, residual moisture, and freezing rate, can affect the stability of the active components during the frozen storage of foods, pharmaceuticals, and organisms. Cryoprotectants are effective for protecting cells from freezing damage. Dimethyl sulfoxide (DMSO) and glycerol are the most widely used cryoprotectants, however, their high doses can be toxic to the cells (Hasan et al., 2018). Hence, it is crucial to screen suitable cryoprotectants to improve bacterial survival ratio and maintain enzymatic activity.

Several scholars have investigated EPS-producing bacteria in sediments of different seas. *Pseudoalteromonas* sp. MD12-642 was isolated from Madeira Archipelago sediments and its EPS had a high molecular weight of 1000 kDa (Roca et al., 2016). Further, *Colwellia psychrerythraea* 34H was isolated from subzero Arctic sediments and its EPS displayed improved freeze protection (Casillo et al., 2017). Wei et al. (2021) isolated *Bacillus* sp. H5 from South China Sea sediments and reported that EPS could be utilized as an immune adjuvant. Furthermore, *Bacillus* sp. can effectively secrete EPS, which is considered a significant antioxidant (Pei et al., 2020). Isolation of EPS-producing bacteria and investigation of the structure and properties of EPS has recently gained popularity among researchers.

However, to the best of our knowledge, there are no studies on EPS-producing bacteria collected from Western Pacific sediments. In this work, we explored the structure and properties of EPS secreted by *Bacillus* sp. AP-4 from deep-sea sediments. EPS yield was optimized by changing external conditions and further purified by the Cellulose and Sepharose column. The structural characterization of EPS was done by High-Performance Liquid Chromatography (HPLC), one-dimensional $^{1}H$ and $^{13}C$ Nuclear Magnetic Resonance (NMR), Fourier-transform infrared (FTIR) analysis, Scanning electron microscopy (SEM), and X-ray photoelectron spectrometer (XPS) analysis. Further, the properties of EPS were investigated by thermogravimetry (TG), differential scanning calorimetry (DSC), gel permeation chromatography (GPC), and emulsification experiment. Finally, the dual-activity of EPS was established by the antioxidant test and freeze protection test. Moreover, our work also provides a reference value for the exploration of the structure and properties of EPS produced by deep-sea bacteria.

# Materials and methods

## Biochemical reagents and medium

Molecular biology reagents were purchased from BGI Co., Ltd. (Beijing, China). All chemical reagents were purchased from Sinopharm Group Co., Ltd. (Shanghai, China). Luria-Bertani (LB) medium contained (g $L^{-1}$): NaCl 10.0, yeast powder 5.0, peptone 10.0 and pH 7.2. LB solid medium was formed by adding 20 g $L^{-1}$ agar to the LB medium. 2216E modified medium contained (g $L^{-1}$): yeast powder 1, peptone 5.0, ferric citrate 0.1, NaCl 20, $MgCl_2{\cdot}6H_2O$ 12.8, $Na_2SO_4$ 3.24, $CaCl_2$ 1.8, KCl 0.55, $Na_2CO_3$ 0.16, $(NH_4)_2SO_4$ 0.0016, $Na_2HPO_4$ 0.008, pH 7.5. Minimal salts medium contained (g $L^{-1}$): $Na_2HPO_4$ 1.5, $KH_2PO_4$ 3.48, $(NH_4)_2SO_4$ 4, $MgSO_4$ 0.7, yeast powder 0.01, pH 7.2. All mediums were sterilized at 121°C for 30 min.

## Selecting and identification of deep-sea bacteria

Sediments were derived from the bottom mud of 6,000 m in the Western Pacific Ocean (32°32N, 146°13E). The sediments were suspended in minimal salts medium for 72 h and then inoculated into LB medium for 48 h at 20°C. Next, mixture was diluted and spread on LB solid medium. Strains with large apparent viscosity were chosen for sequential enrichment and cultivation. The extraction and identification of microbial genomes were presented in Section S1 (Supplementary Information).

## EPS extraction and purification from *Bacillus enclensis* AP-4

Strain AP-4 was inoculated in LB medium until logarithmic growth phase and then transferred into 2216E modified medium. Incubation process was implemented under aerobic

conditions at 25°C for 72 h. Extraction steps of crude BPS refer to our previous work (Hu et al., 2021). Briefly, the strain was inoculated in 2216E modified medium and fermented at 25°C for 72 h. The cultures were centrifuged and the supernatant was concentrated about ten times (i.e., volume reduction from 100 to 10 mL) by reduced pressure distillation. And 70% (w/v) trichloroacetic acid (TCA) was added to the cell-free supernatant with a final concentration of 15% (w/v), kept at 4°C overnight, and centrifuged at 11,000 ×*g* and 4°C for 20 min to remove protein. Subsequently, the supernatant was precipitated by mixing with three times volume of pre-cooling 95% (v/v) ethanol and kept at 4°C for 12 h, and BPS was collected with centrifugation at 11,000 ×*g* and 4°C for 20 min. The obtained BPS was dialyzed (8 kDa-14 kDa cut-off, Leibusi, Shanghai, China) in deionized water for 72 h. The crude BPS was obtained after freeze-drying.

Further, the crude BPS was separated by Cellulose column (3.0 × 30 cm) and eluted with gradient concentration of NaCl solutions (0, 0.2, 0.4, 0.6, 0.8 and 1.0 M) at a flow rate of 1 mL $min^{-1}$. Five mL per tube was collected by BSZ-100 auto fraction collector (Shanghai Jiapeng Technology Co. Ltd., Shanghai, China). Next, the content of carbohydrate was determined by phenol sulfuric acid method (Dubois et al., 1956). The fractions of BPS were dialyzed overnight and lyophilized. BPS was further purified by Sepharose column (1.6 × 80 cm) and eluted with ultrapure water at a flow rate of 1 mL $min^{-1}$. Finally, the major fraction was pooled, dialyzed and lyophilized for subsequent analysis.

## Effect of carbon source and physicochemical factors on EPS yield

The strain AP-4 was cultured at different glucose concentration (0-10%, w/v), NaCl concentration (0-24%, w/v), pH (5-10) and temperatures (10-30°C) in 2216E modified medium to investigate the BPS yield. The obtained BPS was weighed on the electronic balance.

## Structural characterization of BPS

### Ultraviolet-visible analysis and monosaccharide composition analysis

The purified BPS was analyzed by an UV-VIS spectrophotometer (T9, Presee, China). Briefly, BPS was dissolved in deionized water to form 1 mg $mL^{-1}$ of solution, and UV-VIS spectrum was recorded in a wavelength ranging from 200-600 nm. Monosaccharide composition of BPS was estimated by HPLC, which referenced our previous work (Hu et al., 2020b). Briefly, the 10 mg of BPS was dissolved in 5 mL of 2 mol $L^{-1}$ trifluoroacetic acid (TFA) and hydrolyzed at 110°C for 2 h. TFA was removed by vacuum evaporation, and solution pH was adjusted to 7.0 with 5 mol $L^{-1}$ NaOH. Monosaccharide standards and acid-hydrolysate of BPS were heated with l-cysteine methyl ester in pyridine at 70°C for 2 h followed by the addition of arylisothiocyanate and reaction for 90 min. The water phase was filtered with a 0.45 μm microporous membrane and then subjected to HPLC injection analysis. The monosaccharide composition was analyzed by a Thermofisher U3000 HPLC system equipped with a WAD detector reversed-phase C18 analytical column (4.6 mm × 250 mm, 5 μm, Agilent Technologies). A mobile phase system consisting of 15% acetonitrile and 85% $KH_2PO_4$ buffer solution (0.1 mol $L^{-1}$, pH 6.7) was used for experimental analysis, and the flow rate was 1 mL $min^{-1}$. The UV spectrophotometric detector wavelength was 245 nm for the derivatized monosaccharides.

### FTIR spectra analysis

The main functional groups of BPS were determined by FTIR spectra. The dried BPS was mixed with KBr and pressed into pellets for FTIR analysis (NICOLET iS10, Thermo Scientific, Waltham, Massachusetts, USA) in the scanning range of 4000 to 400 $cm^{-1}$ at room temperature (25 ± 0.1°C).

### NMR spectra analysis

NMR spectra were used to analyze the positions of anomeric hydrogen and anomeric carbon in sugar chains. In short, the 20 mg of BPS was dissolved in 0.5 mL $D_2O$ (99.9%) and then centrifuged at 11,000 × *g* for 20 min. The supernatant was repeatedly lyophilized three times to fully remove the hydrogen. In the end, BPS was dissolved in $D_2O$ and transferred to the NMR tube. BPS was analyzed by a 600 MHz NMR spectrometer (Bruker Avance IIIHD, Germany) loaded with a 5 mm inverse probe (QXI).

### Microstructure of *Bacillus enclensis* AP-4 and BPS

The surface morphology of strain AP-4 and BPS were observed by our previous method (Hu et al., 2020a). In brief, strain AP-4 was inoculated (2%, v/v) into 2216E modified medium and fermented at 25°C for 72 h. Cells were harvested by centrifugation (8,000 × g, 10 min) and washed three times after 48 h cultivation. Then, cells were fixed by glutaraldehyde and dehydrated. The freeze-dried BPS and dried cells were pasted on copper platform. Microstructure of cells and BPS were observed by SEM (FEI-Verios 460L, Waltham, Massachusetts, USA) with an accelerating voltage of 10 kV.

### XPS analysis

The elemental composition and electronic states of BPS were performed on XPS (Thermo Scientific ESCALAB Xi +, USA) with the Mg Kα (1253.6 eV, 300 W) (Pan et al., 2021).

# Characterization of BPS

## Biochemical composition of BPS

The carbohydrates and protein of BPS were determined by phenol sulfuric acid method and description of Bradford (1976). In short, the 800 μL of Bradford reagent was added and mixed well with 200 μL of 5 mg $mL^{-1}$ BPS. The mixture was incubated at room temperature for 30 min. The absorbance was measured at 595 nm and the protein content was calculated from the standard curve.

## Molecular weight analysis

The weight average molecular weight (Mw) and number average molecular weight (Mn) of BPS were investigated by GPC (Liao et al., 2022). HLC-8320 GPC system (EcoSEC, Tokyo, Japan) equipped a chromatograph column (TSKgel GMPWXL, 7.8 mm × 30 cm, Beijing, China) and refractive index detector (RID-20A, Shimadzu, Tokyo, Japan). The mobile phase was 0.15 mol $L^{-1}$ of $NaNO_3$, and flow rate was 0.6 mL $min^{-1}$ at 40°C. The 1 mg $mL^{-1}$ of BPS and 1 mg $mL^{-1}$ of dextran standards were injected 20 μL. Finally, dextran standards with a molecular weight range of 5-500 kDa were utilized to calculate the Mw and Mn of BPS. The polydispersion index (PDI) was deduced as follows:

$$PDI = Mw / Mn$$

## Thermostability analysis

Thermostability of BPS were measured by simultaneous thermal analysis (STA, 449 F3, Netzsch, Germany). BPS was placed in $Al_2O_3$ crucible and heated from 30 to 800°C at a rate of 10°C $min^{-1}$.

## Emulsification capacity of BPS

Emulsification capacity of BPS was determined our previous description (Hu et al., 2022). The 5 mL of 1 g $L^{-1}$ BPS, Span-20, and Xanthan gum were fully mixed with 5 mL peanut oil, sesame oil, olive oil, corn oil, rapeseed oil, and soybean oil. The mixture was vortexed for 2 min and then stood for 48 h. Emulsification Index (EI) was deduced as the following formula:

$$EI = \frac{He}{Ht} \times 100\ \%$$

Height of emulsification layer and mixture was denoted as *He* and *Ht*, respectively.

# Antioxidant activity of BPS

## DPPH radical scavenging assay

The 2,2-diphenyl-1-picrylhydrazyl (DPPH) radical scavenging activity of BPS was determined as the previous description (Cai et al., 2019). BPS was dissolved in ultrapure water to prepare different solutions (1.0-5.0 mg $mL^{-1}$). The 1 mL of solution was equably mixed with 5 mL of 0.1 mM DPPH solution and then stood for 30 min at room temperature in darkness. The radical scavenging activity was measured the absorbance at 517 nm. Ascorbic acid (Vc) was considered as positive control. DPPH radical scavenging efficiency was deduced as the following equation:

$$\text{DPPH scavenging efficiency (\%)} = [1 - (A_{sample} - A_{control})/A_{blank}] \times 100\ \%$$

where $A_{blank}$ was the absorbance of DPPH, $A_{sample}$ was the absorbance of mixture, and $A_{control}$ was the absorbance of ultrapure water.

## ABTS radical scavenging assay

The 2, 2'-azino-bis(3-ethylbenzothiazoline-6-sulfonic acid) (ABTS) radical scavenging assay is usually used to evaluate the antioxidant capacity of extracts or compounds. ABTS radical scavenging activity of BPS was determined by the previous method with some modifications (Ma et al., 2018). In brief, equal volumes of ABTS solution (7.00 mM) and $K_2S_2O_8$ solution (2.50 mM) were homogeneously mixed and incubated for 12 h under dark condition at room temperature. Then, the mixture was diluted with an ethanol to prepare the ABTS working solution. Then, 1 mL of ABTS working solution was added to the 1 mL BPS solutions (1.0-5.0 mg $mL^{-1}$). The mixture was stood for 30 min at room temperature and measured the absorbance at 734 nm. ABTS scavenging efficiency was deduced as the following equation:

$$\text{ABTS scavenging efficiency (\%)} = [1 - (A_{sample} - A_{control})/A_{blank}] \times 100\ \%$$

Where $A_{blank}$ was the absorbance of ABTS working solution, $A_{sample}$ was the absorbance of mixture, and $A_{control}$ was the absorbance of ultrapure water.

## Hydroxyl radical scavenging assay

Hydroxyl radical scavenging capacity is an essential indicator for antioxidant capacity of substances, which referenced the method of Zhang et al. (2022). Briefly, equal volumes of $FeSO_4$ solution (10 mM), salicylic acid solution (10 mM), $H_2O_2$ solution (10 mM) and BPS solutions (1.0-5.0 mg $mL^{-1}$) were equably mixed and incubated at 37°C for 30 min. The absorbance of mixture was measured at 510 nm. Hydroxyl radical scavenging efficiency was deduced as the following equation:

$$\text{Hydroxyl radical scavenging efficiency (\%)} = [1 - (A_{sample} - A_{control})/A_{blank}] \times 100\ \%$$

where $A_{blank}$ was the absorbance of mixture ($FeSO_4$, salicylic acid solution and $H_2O_2$ solution) without BPS, $A_{sample}$ was the absorbance of mixture with BPS, and $A_{control}$ was the absorbance of ultrapure water.

### Superoxide anion radical scavenging assay

Superoxide anion radicals, as a type of free radical generated by metabolism of living organisms, can attack biological macromolecules such as lipids, proteins and fatty acids thus causing the damage of cell structure and function (Jie et al., 2022). The superoxide anion radical scavenging activity was assessed by the previous method (Yang et al., 2022). In brief, 1 mL of BPS solution (1.0-5.0 mg $mL^{-1}$) and 5 mL Tris-HCl (50 mM, pH 8. 2) buffer was mixed and incubated at 25°C for 30 min. Then, 1 mL of pyrogallic acid (7 mM) was added to mixture and shocked for 5 min. Eventually, a drop of concentrated hydrochloric acid (10 M) was used to stop the reaction. The absorbance of sample was measured at 320 nm and Vc was used as the positive control. The superoxide anion radicals scavenging efficiency was deduced as the following equation:

$$\text{Superoxide anion radicals scavenging efficiency (\%)} = [1 - (A_{sample} - A_{control})/A_{blank}] \times 100\ \%$$

where $A_{blank}$ was the absorbance of pyrogallic acid, $A_{sample}$ was the absorbance of mixture, and $A_{control}$ was the absorbance of ultrapure water.

## Evaluation of cytoprotective activity

### Determination of cell viability

Determination of cell viability were measured by the method of Dimopoulou et al. (2016) with some modification. The representative Gram-negative bacteria (*Escherichia coli* DH5a) and Gram-positive bacteria (*Staphylococcus aureus* ATCC25923) were selected for the investigation of cell viability. The 50 mL of *E. coil* and *S. aureus* culture broth in logarithmic growth phase ($OD_{600}$≈1.8) were centrifuged (10,000 × *g*, 10 min, 4°C). Then, cells were washed twice with sterile water and centrifuged again. BPS was dissolved in sterile water to prepare different concentration (0.5, 1.0, 1.5, 2.0 and 2.5%, w/v). The 0.8 mL of BPS solutions and cells were mixed and frozen at -80°C for 7 d. Equal volumes of 20% glycerol and sterile water were used as positive control and negative control, respectively. Finally, the frozen cells were inoculated into LB medium and cultured at 30°C for 36 h. Then, 200 μL of suspension was coated on LB solid medium to examine the cell survival ratio. Each sample was repeated three times. The cell survival ratio was calculated by the following equation:

$$\text{Cell survival ratio (\%)} = N_A/N_B \times 100\ \%$$

where $N_A$ was the number of cells after freezing (CFU/mL); $N_B$was the number of cells before freezing (CFU/mL).

### $Na^+/K^+$-ATPase activity assay

$Na^+/K^+$-ATPase activity of cells was determined by $Na^+/K^+$-ATPase activity kit from Solarbio Science & Technology Co. (Beijing, China). The content of enzyme activity was defined as Units/$10^4$ cells.

## Statistical analysis

One-way analysis of variance (ANOVA) was adopted to analyze all data, relying on SPSS v22.0 (SPSS Inc., Chicago, IL, USA). Statistical significance was determined by Duncan's multiple-range tests. $p < 0.05$ was considered statistically significant. In all cases, experiments were performed in triplicates (n = 3).

# Results and discussion

## Isolation and identification of an EPS-producing bacteria

A total of eight culturable bacteria were isolated from the deep-sea sediment after continuous isolation and purification. Three strains with large apparent viscosity were named AP-4, BP-1, and BP-2, respectively, and were selected to measure the EPS yield. EPS yields of strains AP-4, BP-1, and BP-2 were 3.256, 2.485, and 2.793 g $L^{-1}$ in the 2216E modified medium, respectively. Strain AP-4 secreted maximum EPS, so it was regarded as the target strain for the subsequent identification.

Strain AP-4 was a Gram-positive bacterium and was non-motile and long rod-shaped. The colonies were yellow and the edges were intact on LB solid medium (Figure 1B). Besides, the colonies were opaque and round, and the bulge on the surface was shiny. Notably, colony size was only 0.8–2.2 μm (Figures 1C, D). Figure 1A shows that strain AP-4 had the highest similarity (100%) to *Bacillus enclensis* SGD-1123 (GenBank accession No. NR_133700.1). Based on the results of the phylogenetic tree and sequence alignment, the strain was designated as *Bacillus enclensis* AP-4 (GenBank accession No. ON159709).

## Optimization of EPS yield

Deep-sea bacteria are mostly salt-tolerant, which enables their expected growth and metabolism (Anburajan et al., 2021). Figure 2A shows the effect of NaCl concentration on the EPS yield and the growth of strain. The Strain AP-4 could grow in the range of 0–24% NaCl ($OD_{600}$>0.5), and the growth of strain

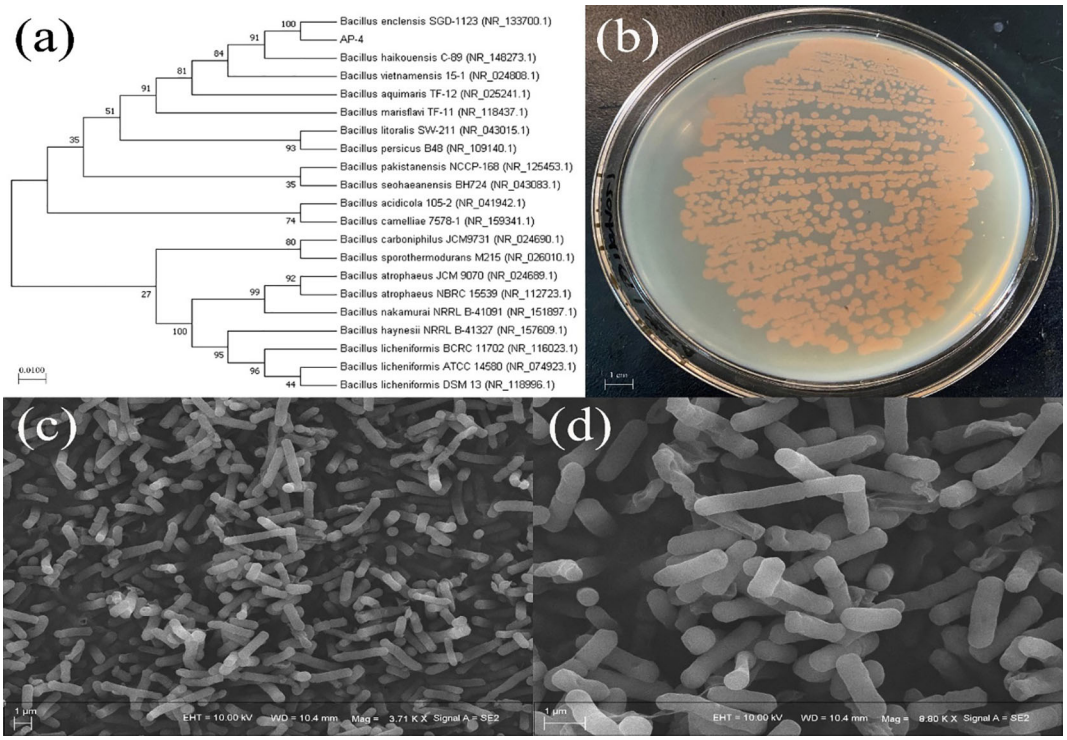


FIGURE 1
Phylogenetic tree of strain AP-4 and the related twenty strains by Neighbor-joining method **(A)** Image of strain AP-4 on LB solid medium **(B)** SEM image magnified 3710 times **(C)** SEM image magnified 8800 times **(D)**.

exhibited an increasing trend followed by decrement with increasing salinity. Furthermore, the highest yield of EPS appeared at 9% NaCl and was estimated to be 3.59 ± 0.11 g $L^{-1}$. Moreover, bacteria usually accumulate active substances inside the cells or secrete EPS outside the cells to assist themselves against environmental stress (Hu et al., 2020a). The external stress induces the strain to secrete more EPS, which avoids cellular damage. Therefore, the presence of a certain amount of NaCl was beneficial to increasing the EPS yield.

The microorganisms mainly use two carbon sources, glucose and sucrose, to synthesize EPS (Freitas et al., 2017). Several research groups have reported that *Bacillus* sp. utilizes glucose to produce EPS. The growth of strain gradually decreased with the increase in the concentration of glucose (Figure 2B). It was noteworthy that EPS yield reached the highest value (3.86 ± 0.30 g $L^{-1}$) at a glucose concentration of 2%. In a similar study, Wagh et al. reported that *Bacillus* sp. SGD-03 produced 2.16 g $L^{-1}$ EPS in nutrient broth containing 2% glucose (Wagh et al., 2022). Furthermore, *Bacillus licheniformis* isolated from the thermal fluid sample can secrete 165 mg $L^{-1}$ EPS in MD 162 minimal medium containing 0.6% glucose (Caccamo et al., 2020).

Microorganisms are sensitive to the variation of pH and prefer to survive in neutral or alkaline conditions, and not acidic conditions (Jia et al., 2022). Figure 2C shows strain AP-4 had a wide pH tolerance range (pH 5-10), allowing it to tolerate the superacid or peralkalic conditions (Figure 2C). In addition, the maximum yield of EPS reached 3.97 ± 0.17 g $L^{-1}$ at pH = 7. The previous reports have shown that the optimum pH for EPS produced by *Antrodia camphorata* was 5.0, and the yield reached 5.05 mg $g^{-1}$ (Shu and Lung, 2004).

Our previous study demonstrated the regulatory role of temperature on the secretion of EPS, hence, the synthesis of specific EPS requires incubation at a specific temperature (Hu et al., 2021). Further, it was found that temperature affected the EPS yield secreted by *Streptococcus thermophilus* strains DGCC7785 and St-143 (Khanal and Lucey, 2018). Figure 2D displays that strain AP-4 displayed growth in the range of 10–30°C. The EPS yield did not vary drastically with temperature variation, and the maximum yield was 4.23 ± 0.17 g $L^{-1}$ at 15°C. Moreover, the optimal fermentation of EPS was 9% NaCl, 2% glucose, pH=7, and 15°C. The EPS produced by *Bacillus enclensis* AP-4 was called BPS.

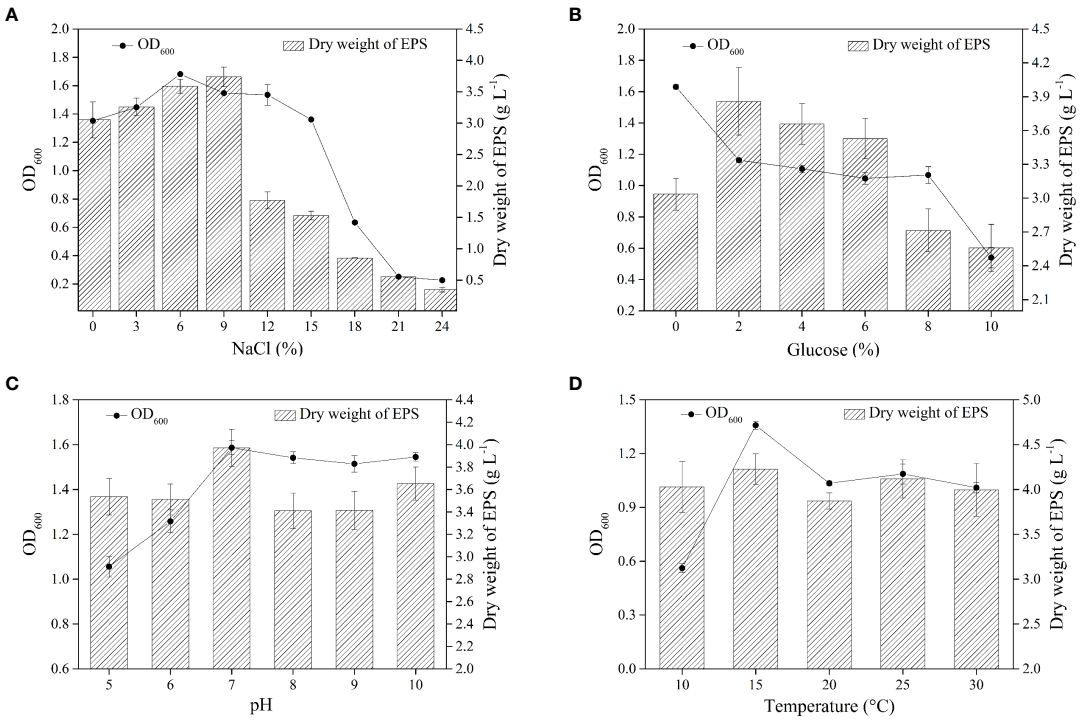


FIGURE 2
The effect of single factor optimization on EPS yield. The effect of NaCl on EPS yield at 25°C, 0% Nacl and pH=7 **(A)** The effect of glucose on EPS yield at 25°C, 9% NaCl and pH=7 **(B)** The effect of pH on EPS yield at 25°C, 9% NaCl and 2% glucose **(C)** The effect of pH on EPS yield at 9% NaCl, 2% glucose and pH =7 **(D)**.

## Purification of crude BPS

The preliminary separation and decolorization of crude BPS were carried out on the Cellulose column. Figure 3A shows three sharp peaks suggesting successful elution of BPS-1, BPS-2, and BPS-3 with different concentrations of NaCl solution. The neutral polysaccharide was eluted with distilled water, while the acidic polysaccharide was eluted with a NaCl solution. Moreover, previous reports have described the potential antioxidant activity of acidic polysaccharides (Yuan et al., 2019). The main fraction appeared in the eluate of 0.8 M NaCl and was pooled, dialyzed, and freeze-dried for further purification. The sample was further purified through a Sepharose column, and a single peak suggests the purification of BPS (Figure 3B). Further, the purified BPS solutions were collected, dialyzed, and freeze-dried for structure and properties analysis.

## Structural characterization of BPS

### UV-VIS analysis

UV-VIS spectrum of the purified BPS was recorded (Figure S1). The maximum absorption of purified BPS was obtained at 220 nm, which is a characteristic absorption peak of carbohydrates. Moreover, there were no absorption peaks at 260 nm and 280 nm, indicating the absence of protein and nucleic acid in the sample. Furthermore, the result demonstrates that BPS was effectively purified. Several researchers had also reported similar purification results (Wang et al., 2020; Kumar et al., 2022).

### Monosaccharide composition analysis

Figures 3C, D shows the HPLC analysis of the monosaccharide composition of BPS. Similarly, the retention time of standard monosaccharides and BPS was demonstrated (Tables S1, S2). BPS hydrolysates displayed peaks at 13.78, 15.97, 27.66, 31.46, and 32.62 min, corresponding to mannose, glucosamine, glucose, galactose, and xylose, respectively. The content of mannose was higher than other monosaccharides components, while xylose was the least. Moreover, the molar ratio of mannose, glucosamine, glucose, galactose, and xylose was 1.00: 0.09: 0.04: 0.09: 0.07. Wei et al. reported that EPS5SH produced by *Bacillus* sp. H5 was composed of Man, GlcN, Glc, and Gal in a molar ratio of 1.00: 0.02: 0.07: 0.02 (Wei et al., 2021).

### FTIR spectra analysis

FTIR spectroscopy was employed for the analysis of the functional groups of BPS (Figure S2). The peaks at 3550 $cm^{-1}$

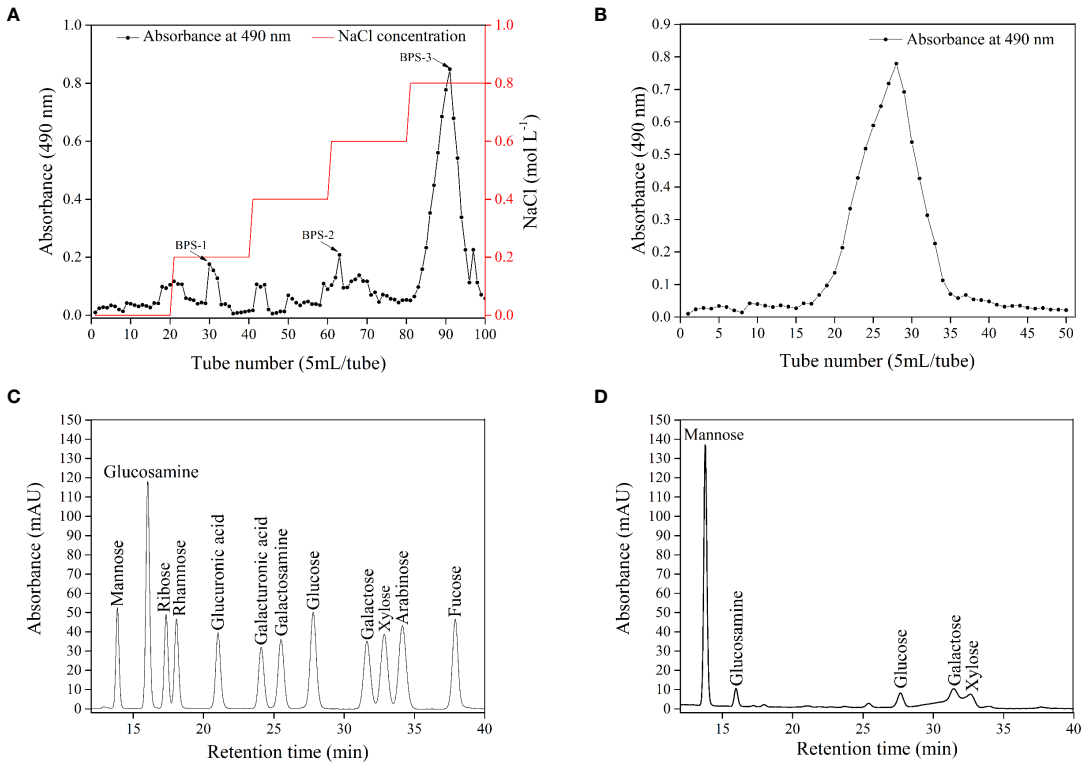


FIGURE 3
Elution profile of crude BPS on Cellulose column **(A)** and Sepharose column **(B)**. HPLC chromatograms of standard monosaccharide **(C)** and BPS **(D)**.

and 3408 $cm^{-1}$ could be attributed to the amino and hydroxyl groups (Ashraf et al., 2022; Kailasam et al., 2022). Further, the peaks at 1687 and 1620 $cm^{-1}$ could be ascribed to the presence of the C=O group (Wang et al., 2013). A strong peak at 1132 $cm^{-1}$ indicated the presence of α-(1→4) glycosidic linkages (Lee et al., 2007). The peak at 671 $cm^{-1}$ was attributed to the existence of the C-C=O group (Wiercigroch et al., 2017). Furthermore, the peak at 605 $cm^{-1}$ displayed the vibrations of pyranose rings (Mitić et al., 2009). The hydroxyl and amino groups in BPS facilitate the realization of the reductive properties.

## NMR spectra analysis

NMR was used to explore the structural characteristics of BPS (Figure 4). Figure 4A shows the proton signal of H2-H6 that appeared between chemical shifts 3 and 4. Further, the $^{1}H$ NMR spectrum showed seven anomeric proton signals at 5.22, 5.07, 5.04, 5.02, 4.97, 4.89, and 4.82 ppm, explaining that BPS contained α and β-configuration sugar residues. Similarly, five anomeric carbon signals were also present at 103.01, 102.19, 100.56, 99.98, and 98. 20 ppm, respectively (Figure 4B). All sugar residues were pyranose rings, which could be deduced due to the absence of signal in the region of 82–88 ppm. Furthermore, BPS did not contain uronic acid, which was also supported by the absence of signal (δ > 170 ppm). There was no found δ< 20 ppm, elaborating the absence of fucose and rhamnose. The NMR results were in reasonable agreement with HPLC and FTIR data.

## Microstructure of BPS

The SEM micrographs of BPS exhibited a rod-like structure and a rough surface (Figure 5). Each bar structure was sufficiently stacked indicating sufficient toughness of BPS. EPS secreted by marine *Bacillus* sp. exhibited a fibrous network structure with a relatively smooth surface (Wagh et al., 2022). EPS produced by probiotic *Bacillus licheniformis* AG-06 showed uneven smooth surfaces with a network-like structure (Vinothkanna et al., 2021). Furthermore, our previous research reported that EPS also represented the network structure (Hu et al., 2021). However, the microstructure of BPS is rare in *Bacillus* sp. Moreover, the rough surface and sufficient toughness can be employed as plasticized biofilm materials (Saravanan and Shetty, 2016), which prove more stable compared to the other microscopic material. Further, the rod-like structure can form hydrated polymers to increase the water retention ability and solubility of products, impelling their more competitive potential in the food, pharmaceutical, and cosmetic industries.

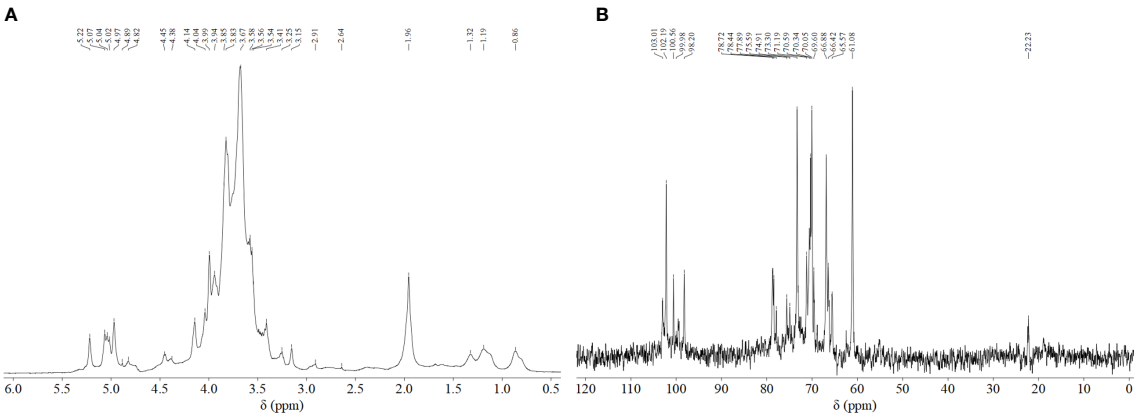


FIGURE 4
NMR spectra of the BPS: **(A)** $^{1}$H NMR spectrum; **(B)** $^{13}$C NMR spectrum.

## XPS analysis

XPS analysis was used to verify the properties of functional groups. The wide spectra revealed that BPS contained 70.15% C, 2.41% N, and 27.44% O (Figure 6A). The trace elements such as S and P accounted for less than 1%, indicating that C, N, and O were predominantly present in BPS. Figures 6B-D exhibits the high-resolution spectra of C, N, and O. In the high-resolution spectrum of C1s, peaks at 287.2, 284.7, and 283.2 eV could be attributed to the C=O, C-OH, and C-(C/H) group (Li et al., 2017; Moreira et al., 2017). Further, the N1s peaks at 397.9 eV formed the amino nitrogen (N-H), explaining the presence of the amino group (Safaei et al., 2018). The O1s peak at 531.7 and 530.5eV belonged to the C=O and C-O (Puziy et al., 2008). These results are in good agreement with FTIR analysis.

# Characterization of BPS

## Biochemical composition and Mw of BPS

The total carbohydrate and protein content in BPS were measured to be 96.18 ± 0.36% and 1.67± 0.18% (w/w). The higher content of carbohydrates indicates wider applications of the exopolysaccharide. Analogously, the quantity of carbohydrate and protein were found to be 96.10 ± 0.2% and 58.3 ± 0.02% in EPS (Shankar et al., 2021). Asgher et al. reported the production of EPS by *Bacillus licheniformis* (2.855 g $L^{-1}$), and the total carbohydrate content was 87.3% (Asgher et al., 2021). The BPS isolated in the present study had more carbohydrates and less protein suggesting its potential application in industries such as cosmetics.

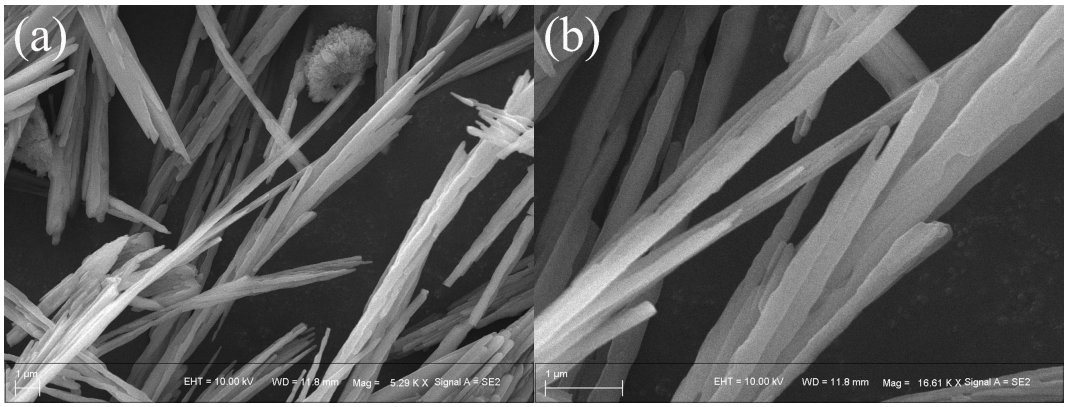


FIGURE 5
SEM images of BPS. SEM image magnified 1,000 times **(A)** and 5,000 times **(B)**.

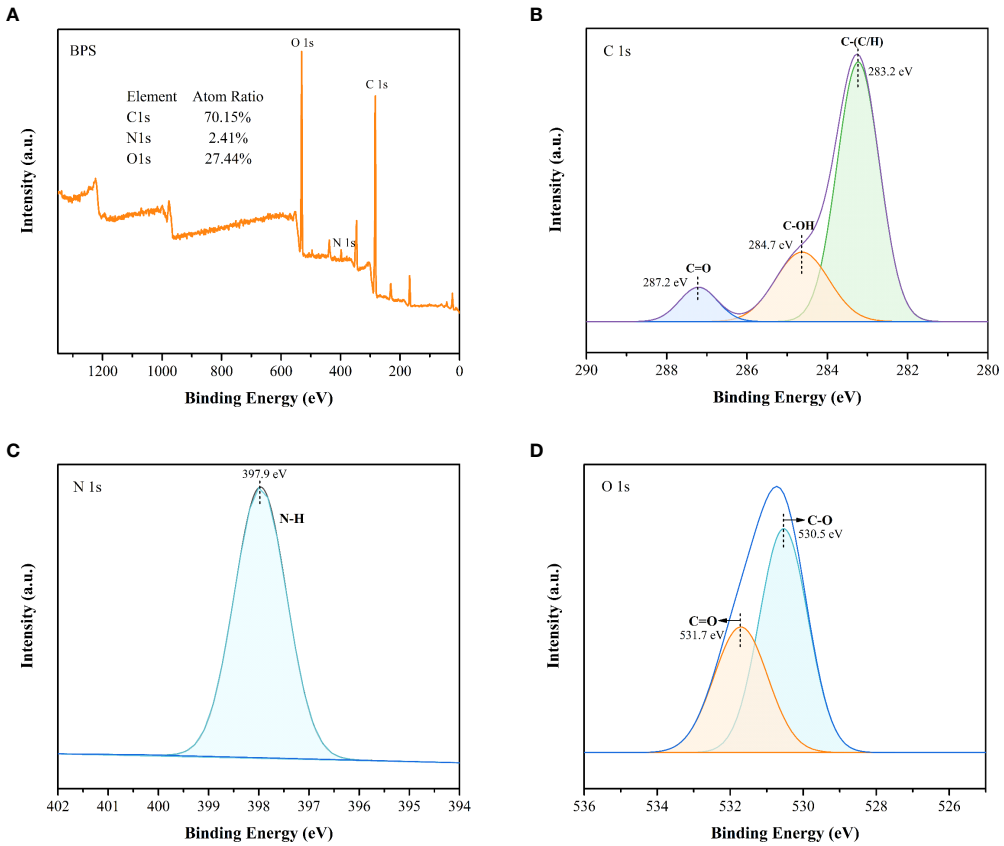


FIGURE 6
The wide spectra **(A)** and high-resolution XPS peaks of C1s **(B)**, O1s **(C)**, and N1s **(D)**.

The Mw of EPS is the most influential parameter affecting their biological activity. The Mw of BPS was examined by GPC, and the result indicated a single peak (Figure S3). The Mw and Mn of BPS were estimated to be 23,434 and 7,601 Da. Furthermore, the PDI of BPS was 3.08, which elaborated that BPS was a dispersed state.

## Thermal behavior of BPS

The thermostability of EPS is fundamental for its application in the food industry (Abid et al., 2019). Figure 7A shows two different steps of TGA. In the first stage, a weight loss of 2.40% was recorded at 107.83°C, which could be attributed to the loss of residual water in polysaccharides (Wang et al., 2010). In the second stage, the depolymerization of BPS resulted in a weight loss of 28.13% from 107.83°C to 798.16°C, due to the breaking of the chemical bonds. Finally, only 69.36% of BPS remained at 798.16°C as the weight loss plateaued. Furthermore, the degradation process of EPS was observed from the DTG curve. The peak at 130.5°C was regarded as degradation temperature (Td), as weight loss was most rapid at that temperature. The Td of BPS was smaller than the previously reported EPS (Rani et al., 2017). DSC was used to characterize the thermal transition of BPS. BPS demonstrated an amorphous to crystalline transition (Tc) temperature at 134.17°C, which was slightly lower than EPS DU10 (Venkatesh et al., 2016). Subsequently, the melting transition of BPS started at 145.33°C, which was higher than some previously studied EPS (Wang et al., 2010). Furthermore, BPS revealed distinct endothermic peaks at 705.67°C. BPS displayed high thermal stability, suggesting its potential application in food or hydrocolloid industries.

## Emulsification capacity of BPS

Emulsification capacity is employed to evaluate the capacity of two insoluble liquids to establish a stable liquid dispersion system under certain conditions. Additionally, emulsification stability also reflects emulsification capacity. BPS exhibited excellent hydrophilicity and formed stable emulsions between the aqueous and oil phases. We explored the emulsification capacity of BPS with six oils i.e., peanut oil, sesame oil, olive oil, corn oil, rapeseed oil, soybean oil, and Span-20, and xanthan gum was used as the control group. Figure 7B shows the excellent emulsification capacity of BPS with EI values greater than 60% in all six tested oils. The highest EI

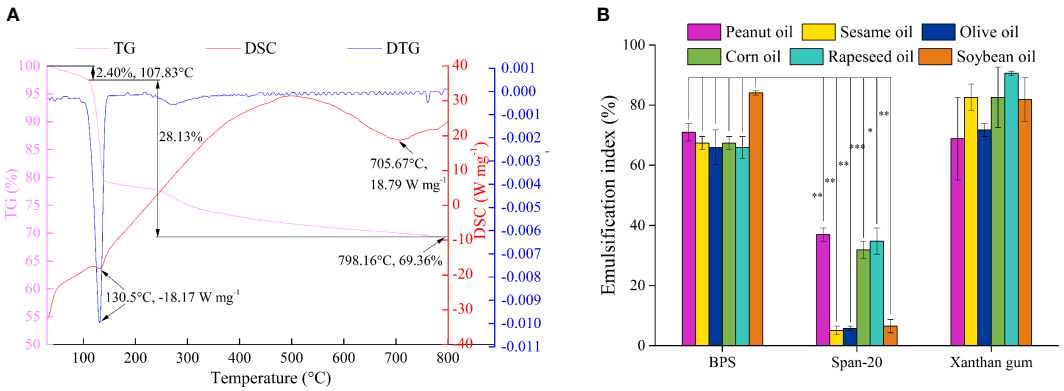


FIGURE 7
The TG (pink line), DSC (red line) and DTG (blue line) curves of BPS **(A)**. Emulsification performance of BPS, Span-20, and Xanthan gum in peanut oil, sesame oil, olive oil, corn oil, rapeseed oil, and soybean oil **(B)**. All values are mean values (n = 3) (*P < 0.05, **P < 0.01, ***P < 0.001).

was found in soybean oil, which presented as 84.06 ± 0.72%. Although xanthan gum displayed a strong emulsification capacity in all six tested oils, the emulsification performance of BPS was significantly higher than Span-20 (∗P< 0.05). Many emulsification experiments on EPS utilize edible oil as the oil phase, such as EPS produced by *Pseudomonas fluorescens* presented the highest emulsification for diesel and olive oil (>50%) (Vidhyalakshmi et al., 2018). Kodali et al. reported EPS from *Bacillus coagulans* RK-02 that exhibited better emulsification activity in sunflower oil than in mustard oil, soybean oil, castor oil, and rice oil (Kodali et al., 2009). The molecular structure, Mw, and functional groups of EPS has substantial effects on emulsification performance. BPS has a strong emulsification capacity, which may be ascribed to the interaction between hydrophilic groups and electrostatic interaction (Yang et al., 2022). Moreover, the formed emulsion was stable for one month (Figure S4), which suggests the employment of BPS for the preparation of oil/water emulsions in the food and cosmetic industries.

## Antioxidant activity of BPS

Figure 8 displays the antioxidant activities of BPS under different stress responses. The scavenging efficiency of Vc for DPPH was better than BPS, and BPS exhibited dose-dependent scavenging efficiency in the range of 1–5 mg $mL^{-1}$ (Figures 8A-D). Figure 8A shows that the highest scavenging efficiency of BPS was achieved up to 83.1 ± 1.9% at 5 mg $mL^{-1}$. Interestingly, only 1 mg $mL^{-1}$ of BPS has demonstrated an extremely strong scavenging efficiency (>60%). Although previous reports had explored the DPPH scavenging efficiency of EPS produced by *Bacillus* sp. (Hu et al., 2019; Gangalla et al., 2021). However, the scavenging efficiency of BPS was recorded to be higher at the same concentration. Furthermore, ABTS scavenging efficiency gradually increased in a dose-dependent manner for Vc and BPS. BPS exhibited 80.3 ± 1.5% of ABTS scavenging efficiency at the highest concentration (5.0 mg $mL^{-1}$) (Figure 8B). Moreover, an excellent scavenging efficiency at the lowest dose (>55%) was demonstrated. EPS secreted by *Bacillus licheniformis* AG-06 showed 70.99% ABTS scavenging efficiency at a concentration of 3mg $mL^{-1}$ (Vinothkanna et al., 2021). ABTS clearance percentage of CPS produced by *Bacillus velezensis* SN-1 exceeded 50.0% when the concentration was 6.0 mg $mL^{-1}$ (Cao et al., 2020). Moreover, hydroxyl radicals and superoxide anion radical scavenging efficiencies were also increased to 74.6 ± 1.1% and 87.5 ± 1.2% with increasing concentration of BPS, respectively (Figures 8C, D). However, the hydroxyl radical scavenging efficiency of BPS was weak at the low concentrations (1 mg $mL^{-1}$), which may be related to its structure. In a similar study, BL-P1 and BL-P2 produced by *Bacillus licheniformis* to scavenge hydroxyl radicals reached 50.07% and 65.13% at 120 μg $mL^{-1}$, respectively (Xu et al., 2019). Furthermore, the presence of hydroxyl groups (-OH) in polysaccharides can promote binding to hydroxyl radicals, thereby enhancing the scavenging efficiency (Zhao et al., 2018). In addition, it has been demonstrated that acidic polysaccharides have superior superoxide anion scavenging activity than neutral polysaccharides (Xu et al., 2011). Further, various functional groups (e.g., C=O, C-O-C, and C-O) maybe involved in the biological activity of EPS (Farinazzo et al., 2020). BPS had displayed better quenching activities against hydroxyl radical and superoxide anion radical compared with the previous EPS reports.

## Evaluation of cytoprotective activity

Figure 9 shows the cryoprotective effect of BPS on *E. coli* and *S. aureus* using 20% glycerol as the positive control and sterile water as the negative control. *E. coli* containing 20% glycerol exhibited the highest survival ratio (95.29 ± 1.24%) after being frozen for 7 d (Figure 9A). In contrast, sterile water maintained only 81.44 ± 2.60% of cell survival ratio. Moreover, the cell survival ratio of *E. coli* decreased with the increase in BPS concentration (2.0–2.5%),

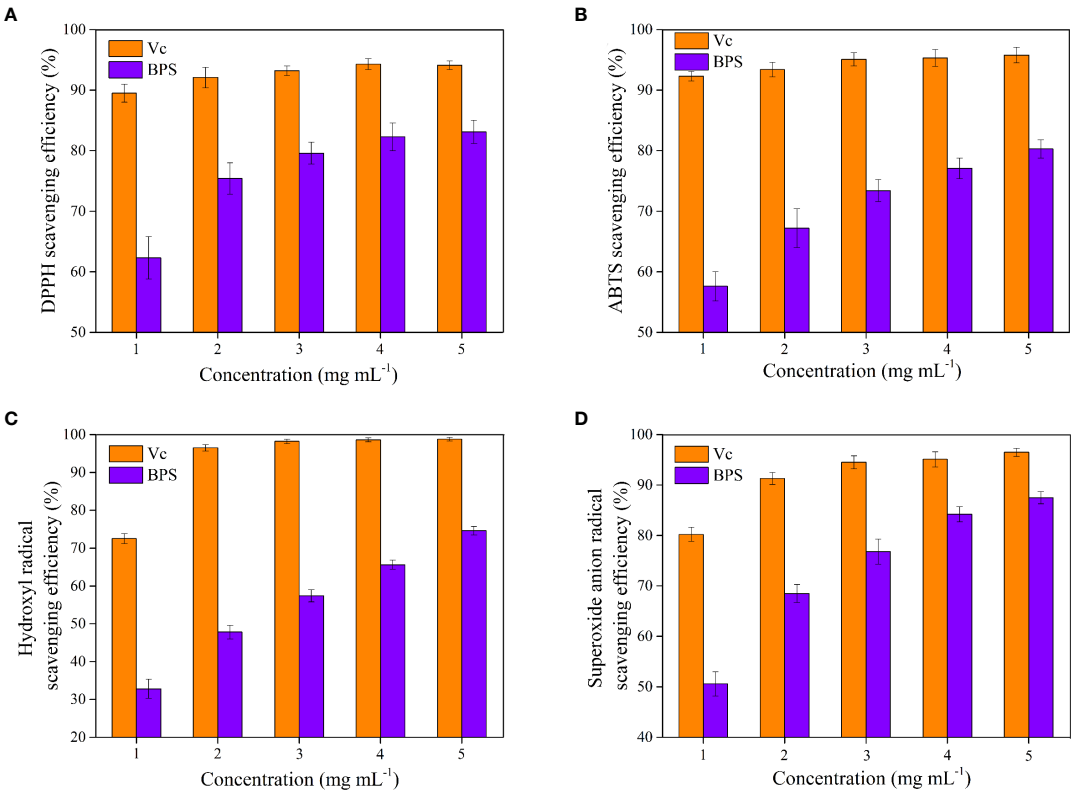


FIGURE 8
Antioxidant activities of BPS *in vitro*. DPPH scavenging activity **(A)**; ABTS scavenging efficiency **(B)**; Hydroxyl radical scavenging efficiency **(C)**. Superoxide anion radicals scavenging efficiency **(D)**. All values are mean values (n = 3).

which may be attributed to the bacteriostatic effect of BPS. The highest survival ratio (95.22 ± 1.86%) was presented at 0.5% BPS, which was a 13.78% increase compared with the sterile water. Likewise, *S. aureus* with 20% glycerol displayed the highest survival rate (96.87 ± 0.85%) after being frozen for 7 d (Figure 9B). On the contrary, the cell survival ratio of *S. aureus* did not significantly decrease with the increase of BPS concentration. The highest survival ratio (96.66 ± 1.26%) was presented at 1.5% BPS, which reflected a 14.58% increase compared with the sterile water. BPS provided a certain level of cryoprotective effect against Gram-positive as well as Gram-negative bacteria. Moreover, previous studies had reported the cryoprotective effect of EPS on other microorganisms (Carrión et al., 2015; Ali et al., 2021). Additionally, as a common cryoprotectant, DMSO and methanol are harmful to cells at high concentrations, while EPS with biodegradability and biocompatibility is relatively safe (Guerreiro et al., 2020). Cryopreservation of cells is a common technique in biotechnology, and BPS with cryoprotective effects can be explored as a cryoprotectant in cosmetics and pharmaceutical domains.

Further, $Na^+/K^+$-ATPase is a special protein in the cell membrane that can break down the ATP to obtain energy. It mainly balances the concentration difference between $K^+$ and $Na^+$ ions inside and outside the cell membrane, thus maintaining the cellular osmotic pressure. The unfrozen *E. coli* showed high $Na^+/K^+$-ATPase activity (Figure 9C). The 20% glycerol also protected the cells to some extent. The low concentration of BPS (0.5–1.5%) well protected the cells and stabilized their enzymatic activity. However, the high concentration of BPS (2.0–2.5%) restricted the growth of bacteria and thus inhibited the activity of $Na^+/K^+$-ATPase. In the same way, different concentrations of BPS all well protected *S. aureus*, and its enzymatic activity tended to be stable (Figure 9D). They had only 40.11% and 53.63% of the initial enzymatic activity for *E. coli* and *S. aureus* without cryoprotectants. Therefore, as a cryoprotectant, BPS can also maintain the enzymatic activity of cells.

## Conclusions

To the best of our knowledge, this is the first report on EPS derived from *Bacillus* sp. isolated from Western Pacific sediments. BPS produced by *Bacillus enclensis* displayed a maximum yield of 4.23 ± 0.17 g $L^{-1}$ in the 2216E modified medium during 72 h incubation. BPS is composed of mannose, glucosamine, glucose, galactose, and xylose and existed in both α and β-configuration sugar residues. The main functional groups of BPS were found to be

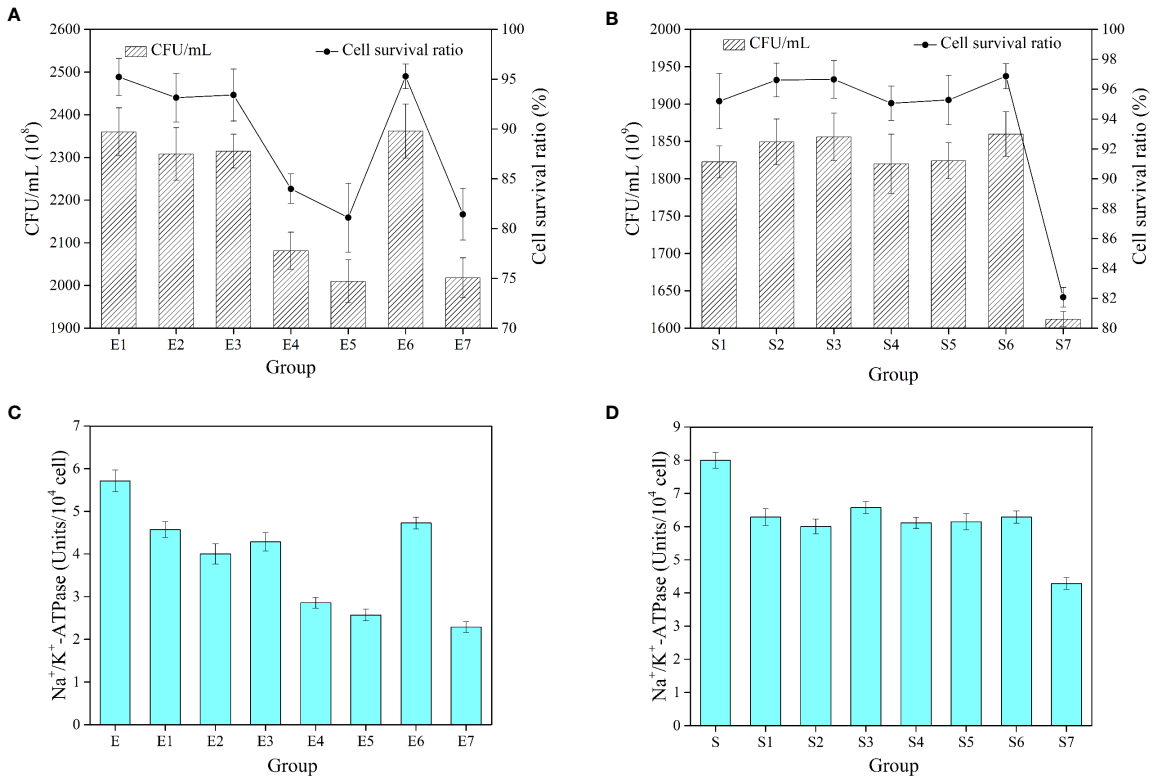


FIGURE 9
The number of cells and cell survival ratio of *E coli* **(A)**. The number of cells and cell survival ratio of *S. aureus* **(B)**. $Na^+/K^+$-ATPase activity in *E coli* after different treatments **(C)**. $Na^+/K^+$-ATPase activity in *S. aureus* after different treatments **(D)**. E represents the unfrozen *E coli*. E1-E7 represent *E coli* supplemented with BPS (0.5, 1.0, 1.5, 2.0 and 2.5%, w/v), 20% glycerol, sterile water and then frozen for 7 d. S represents the unfrozen *S. aureus*. S1-S7 represent *S. aureus* supplemented with BPS (0.5, 1.0, 1.5, 2.0 and 2.5%, w/v), 20% glycerol, sterile water and then frozen for 7 d. All values are mean values (n = 3).

hydroxyl and amino groups. Furthermore, BPS showed a rod-like structure with a rough surface and exhibited high thermal stability and degradation temperature. In addition, BPS displayed excellent hydrophilicity and formed stable emulsions between the aqueous and edible oil phases. BPS revealed excellent performance against DPPH radical, ABTS radical, hydroxyl radical, and superoxide anion radical and provided a certain level of cryoprotective effect against Gram-positive as well as Gram-negative bacteria. The dual-activity of BPS (antioxidant activity and cryoprotective activity) has potential applications in industry and commerce. Exploring the structure and properties of EPS produced by deep-sea bacteria can be exploited by various industries due to its profound practical value.

## Data availability statement

The original contributions presented in the study are included in the article/Supplementary Material. Further inquiries can be directed to the corresponding author.

## Author contributions

XH: designed the study, conducted the experiments, and prepared the manuscript. FL: isolated the strain and extracted the EPS. XZ analyzed the NMR data. YP: launched the cell viability experiment. JL: designed the study. YL: supervised the study. MB: prepared the final manuscript. All authors contributed to the article and approved the submitted version.

## Funding

This study is MCTL Contribution No. 309. It is also supported by the National Natural Science Foundation of China (42277261) and the Fundamental Research Funds for the Central Universities (202161007 and 202072001).

## Acknowledgments

We thank Zhaohui Chen, Xiaotong Xiao, Rong Bi, Qian Liu, Zhaoxia Jiang and Hailong Zhang for technical assistance of the experimental process. We thank Chao Cui, Chuanli Zhang, Minxue Gao, Zhensong Liu and Yulong Guan for sample collection.

## Conflict of interest

The authors declare that they have no known competing financial interests or personal relationships that could have appeared to influence the work reported in this paper.

## Publisher's note

All claims expressed in this article are solely those of the authors and do not necessarily represent those of their affiliated organizations, or those of the publisher, the editors and the reviewers. Any product that may be evaluated in this article, or claim that may be made by its manufacturer, is not guaranteed or endorsed by the publisher.

## Supplementary material

The Supplementary Material for this article can be found online at: https://www.frontiersin.org/articles/10.3389/fmars.2022.976543/full#supplementary-material

## References

Abid, Y., Azabou, S., Joulak, I., Casillo, A., Lanzetta, R., Corsaro, M. M., et al. (2019). Potential biotechnological properties of an exopolysaccharide produced by newly isolated *Bacillus tequilensis*-GM from spontaneously fermented goat milk. *LWT-Food Sci. Technol.* 105, 135–141. doi: 10.1016/j.lwt.2019.02.005

Ali, P., Fucich, D., Shah, A. A., Hasan, F., and Chen, F. (2021). Cryopreservation of cyanobacteria and eukaryotic microalgae using exopolysaccharide extracted from a glacier bacterium *Microorganisms* 9(2) 395. doi: 10.3390/microorganisms9020395

Anburajan, L., Meena, B., Vinithkumar, N. V., and Dharani, G. (2021). Molecular characterization of glycine betaine biosynthesis genes from deep sea halophilic bacteria, *Bacillus atrophaeus* NIOT-DSB21. *Ecol. Genet. Genomics* 18, 100080. doi: 10.1016/j.egg.2021.100080

Andrew, M., and Jayaraman, G. (2020). Structural features of microbial exopolysaccharides in relation to their antioxidant activity. *Carbohydr. Res.* 487, 107881. doi: 10.1016/j.carres.2019.107881

Asgher, M., Rani, A., Khalid, N., Qamar, S. A., and Bilal, M. (2021). Bioconversion of sugarcane molasses waste to high-value exopolysaccharides by engineered *Bacillus licheniformis*. *Case Stud. Chem. Environ. Eng.* 3, 100084. doi: 10.1016/j.cscee.2021.100084

Ashraf, S. S., Parivar, K., Roodbari, N. H., Mashayekhan, S., and Amini, N. (2022). Fabrication and characterization of biaxially electrospun collagen/alginate nanofibers, improved with rhodotorula mucilaginosa sp. GUMS16 produced exopolysaccharides for wound healing applications. *Int. J. Biol. Macromolecules* 196, 194–203. doi: 10.1016/j.ijbiomac.2021.11.132

Bradford, M. M. (1976). A rapid and sensitive method for the quantitation of microgram quantities of protein utilizing the principle of protein-dye binding. *Anal. Biochem.* 72, 248–254. doi: 10.1016/0003-2697(76)90527-3

Caccamo, M. T., Gugliandolo, C., Zammuto, V., and Magazù, S. (2020). Thermal properties of an exopolysaccharide produced by a marine thermotolerant *Bacillus licheniformis* by ATR-FTIR spectroscopy. *Int. J. Biol. Macromolecules* 145, 77–83. doi: 10.1016/j.ijbiomac.2019.12.163

Cai, L. L., Chen, B. H., Yi, F. L., and Zou, S. S. (2019). Optimization of extraction of polysaccharide from dandelion root by response surface methodology: structural characterization and antioxidant activity. *Int. J. Biol. Macromol.* 140, 907–919. doi: 10.1016/j.ijbiomac.2019.08.161

Cao, C. X., Li, Y., Wang, C., Zhang, N. Q., Zhu, X. Y., Wu, R., et al. (2020). Purification, characterization and antitumor activity of an exopolysaccharide produced by *Bacillus velezensis* SN-1. *Int. J. Biol. Macromolecules* 156, 354–361. doi: 10.1016/j.ijbiomac.2020.04.024

Carrión, O., Delgado, L., and Mercade, E. (2015). New emulsifying and cryoprotective exopolysaccharide from antarctic pseudomonas sp. ID1. *Carbohydr. Polymers* 117, 1028–1034. doi: 10.1016/j.carbpol.2014.08.060

Casillo, A., Parrilli, E., Sannino, F., Mitchell, D. E., Gibson, M. I., Marino, G., et al. (2017). Structure-activity relationship of the exopolysaccharide from a psychrophilic bacterium: A strategy for cryoprotection. *Carbohydr. Polymers* 156, 364–371. doi: 10.1016/j.carbpol.2016.09.037

Chen, S. J. Y., Cheng, R., Xu, X. D., Kong, C. C., Wang, L., Fu, R. J., et al. (2022). The structure and flocculation characteristics of a novel exopolysaccharide from a *Paenibacillus* isolate. *Carbohydr. Polymers* 291, 119561. doi: 10.1016/j.carbpol.2022.119561

Costaouëc, T. L., Cérantola, S., Ropartz, D., Ratiskol, J., Sinquin, C., Colliec-Jouault, S., et al. (2012). Structural data on a bacterial exopolysaccharide produced by a deep-sea *Alteromonas macleodii* strain. *Carbohydr. Polymers* 90 (1), 49–59. doi: 10.1016/j.carbpol.2012.04.059

Dimopoulou, M., Bardeau, T., Ramonet, P. Y., Miot-Certier, C., Claisse, O., Doco, T., et al. (2016). Exopolysaccharides produced by *Oenococcus oeni*: From genomic and phenotypic analysis to technological valorization. *Food Microbiol.* 53, 10–17. doi: 10.1016/j.fm.2015.07.011

Dubois, M., Gilles, K. A., Hamilton, J. K., Rebers, P. T., and Smith, F. (1956). Colorimetric method for determination of sugars and related substances. *Anal. Chem.* 28, 350–356. doi: 10.1021/ac60111a017

Farinazzo, F. S., Valente, L. J., Almeida, M. B., Simionato, A. S., Fernandes, M. T. C., Mauro, C. S. I., et al. (2020). Characterization and antioxidant activity of an exopolysaccharide produced by *Leuconostoc pseudomesenteroides* JF17 from juçara fruits (*Euterpe edulis* martius). *Process Biochem.* 91, 141–148. doi: 10.1016/j.procbio.2019.12.005

Feng, X., Gong, Y., Ye, M. Q., and Du, Z. J. (2021). Antibiotic modulation of capsular exopolysaccharide in Pelagicoccus enzymogenes sp. nov. isolated from marine sediment. *Front. Mar. Sci.* 8, 655735. doi: 10.3389/fmars.2021.655735

Freitas, F., Torres, C. A., and Reis, M. A. (2017). Engineering aspects of microbial exopolysaccharide production. *Bioresour. Technol.* 245, 1674–1683. doi: 10.1016/j.biortech.2017.05.092

Gangalla, R., Sampath, G., Beduru, S., Sarika, K., Govindarajan, R. K., Ameen, F., et al. (2021). Optimization and characterization of exopolysaccharide produced by *Bacillus aerophilus* rk1 and its *in vitro* antioxidant activities. *J. King Saud University-Science* 33 (5), 101470. doi: 10.1016/j.jksus.2021.101470

Guerreiro, B. M., Freitas., F., Lima., J. C., Silva., J. C., Dionísio, M., and Reis, M. A. M. (2020). Demonstration of the cryoprotective properties of the fucose-containing polysaccharide FucoPol. *Carbohydr. Polym.* 245, 116500. doi: 10.1016/j.carbpol.2020.116500

Hasan, M., Fayter, A. E. R., and Gibson, M. I. (2018). Ice recrystallization inhibiting polymers enable glycerol-free cryopreservation of microorganisms. *Biomacromolecules* 19 (8), 3371–3376. doi: 10.1021/acs.biomac.8b00660

Hu, X., Fu, H. R., Bao, M. T., Zhang, X. L., Liu, W., Sun, X. J., et al. (2021). Temperature mediates metabolism switching of bacillus sp. AP-3: Analysis of the properties and structure of exopolysaccharides. *Microbiol. Res.* 251, 126839. doi: 10.1016/j.micres.2021.126839

Hu, X., Li, D. H., Qiao, Y., Song, Q. Q., Guan, Z. G., Qiu, K. X., et al. (2020a). Salt tolerance mechanism of a hydrocarbon-degrading strain: Salt tolerance mediated by accumulated betaine in cells. *J. Hazard. Mater.* 392, 122326. doi: 10.1016/j.jhazmat.2020.122326

Hu, X., Li, D. H., Qiao, Y., Wang, X. H., Zhang, Q., Zhao, W., et al. (2020b). Purification, characterization and anticancer activities of exopolysaccharide produced by *Rhodococcus erythropolis* HX-2. *Int. J. Biol. Macromolecules* 145, 646–654. doi: 10.1016/j.ijbiomac.2019.12.228

Hu, X., Pan, Y. P., Bao, M. T., Zhang, X. L., Luo, C. Y., Han, X., et al. (2022). The structure, properties and rheological characterisation of exopolysaccharides produced by *Chryseobacterium cucumeris* AP-2 from deteriorated milk. *Int. Dairy J.* 126, 105253. doi: 10.1016/j.idairyj.2021.105253

Hu, X. Y., Pang, X., Wang, P. G., and Chen, M. (2019). Isolation and characterization of an antioxidant exopolysaccharide produced by bacillus sp. s-1 from sichuan pickles. *Carbohydr. Polymers* 204, 9–16. doi: 10.1016/j.carbpol.2018.09.069

Jia, T. P., Zhang, L., Zhao, Q., and Peng, Y. Z. (2022). The effect of biofilm growth on the sulfur oxidation pathway and the synergy of microorganisms in desulfurization reactors under different pH conditions. *J. Hazard. Mater.* 432, 128638. doi: 10.1016/j.jhazmat.2022.128638

Jie, Z. S., Liu, J., Shu, M. C., Ying, Y., and Yang, H. F. (2022). Detection strategies for superoxide anion: A review. *Talanta* 236, 122892. doi: 10.1016/j.talanta.2021.122892

Jing, L. Y., Zong, S., Li, J. L., Ye, M., Surhio, M. M., and Yang, L. (2017). Potential mechanism of protection effect of exopolysaccharide from *Lachnum* YM406 and its derivatives on carbon tetrachloride-induced acute liver injury in mice. *J. Funct. Foods* 36, 203–214. doi: 10.1016/j.jff.2017.06.057

Kailasam, S., Arumugam, S., Balaji, K., and Kanth, S. V. (2022). Adsorption of chromium by exopolysaccharides extracted from lignolytic phosphate solubilizing bacteria. *Int. J. Biol. Macromolecules* 206, 788–798. doi: 10.1016/j.ijbiomac.2022.03.047

Khanal, S. N., and Lucey, J. A. (2018). Effect of fermentation temperature on the properties of exopolysaccharides and the acid gelation behavior for milk fermented by *Streptococcus thermophilus* strains DGCC7785 and St-143. *J. Dairy Sci.* 101 (5), 3799–3811. doi: 10.3168/jds.2017-13203

Kodali, V. P., Das, S., and Sen, R. (2009). An exopolysaccharide from a probiotic: Biosynthesis dynamics, composition and emulsifying activity. *Food Res. Int.* 42 (5-6), 695–699. doi: 10.1016/j.foodres.2009.02.007

Kumar, A., Mukhia, S., and Kumar, R. (2022). Production, characterisation, and application of exopolysaccharide extracted from a glacier bacterium mucilaginibacter sp. ERMR7:07. *Process Biochem.* 113, 27–36. doi: 10.1016/j.procbio.2021.12.018

Lee, Z., Carder, K., Arnone, R., and He, M. (2007). Determination of primary spectral bands for remote sensing of aquatic environments. *Sensors* 7, 3428–3441. doi: 10.3390/s7123428

Liao, Y. T., Gao, M., Wang, Y. T., Liu, X. Z., Zhong, C., and Jia, S. R. (2022). Structural characterization and immunomodulatory activity of exopolysaccharide from *Aureobasidium pullulans* CGMCC 23063. *Carbohydr. Polymers* 288, 119366. doi: 10.1016/j.carbpol.2022.119366

Li, P., Dou, X. Q., Müller, M., Feng, C. L., Chang, M. W., Frettlöh, M., et al. (2017). Autoinducer sensing microarrays by reporter bacteria encapsulated in hybrid supramolecular-polysaccharide hydrogels. *Macromol. Biosci.* 17 (11), 1700176. doi: 10.1002/mabi.201700176

Ma, W. J., Chen, X. F., Wang, B., Lou, W. J., Chen, X., Hua, J. L., et al. (2018). Characterization, antioxidativity, and anti-carcinoma activity of exopolysaccharide extract from *Rhodotorula mucilaginosa* CICC 33013. *Carbohydr. Polymers* 181, 768–777. doi: 10.1016/j.carbpol.2017.11.080

Mitić, Ž., Nikolić, G. S., Cakić, M., Premović, P., and Ilić, L. (2009). FTIR spectroscopic characterization of Cu(II) coordination compounds with exopolysaccharide pullulan and its derivatives. *J. Mol. Structure* 924-926, 264–273. doi: 10.1016/j.molstruc.2009.01.019

Moreira, G. F., Peçanha, E. R., Monte, M. B. M., Leal Filho, L. S., and Stavale, F. (2017). XPS study on the mechanism of starch-hematite surface chemical complexation. *Miner. Eng.* 110, 96–103. doi: 10.1016/j.mineng.2017.04.014

Pan, Y., Hu, X., Bao, M., Li, Y., and Lu, J. (2021). Fabrication of MIL-Fe(53)/modified g-C3N4 photocatalyst synergy $H_2O_2$ for degradation of tetracycline. *Sep. Purif. Technol.* 279, 119661. doi: org/10.1016/j.seppur.2021.119661

Pei, F. Y., Ma, Y. S., Chen, X., and Liu, H. (2020). Purification and structural characterization and antioxidant activity of levan from *Bacillus megaterium* PFY-147. *Int. J. Biol. Macromolecules* 161, 1181–1188. doi: 10.1016/j.ijbiomac.2020.06.140

Poli, A., Finore, I., Romano, I., Gioiello, A., Lama, L., and Nicolaus, B. (2017). Microbial diversity in extreme marine habitats and their biomolecules. *Microorganisms* 5 (2), 25. doi: 10.3390/microorganisms5020025

Puziy, A. M., Poddubnaya, O. I., Socha, R. P., Gurgul, J., and Wisniewski, M. (2008). XPS and NMR studies of phosphoric acid activated carbons. *Carbon* 46, 2113–2123. doi: 10.1016/j.carbon.2008.09.010

Rani, R. P., Anandharaj, M., Sabhapathy, P., and Ravindran, A. D. (2017). Physiochemical and biological characterization of novel exopolysaccharide produced by *Bacillus tequilensis* FR9 isolated from chicken. *Int. J. Biol. Macromolecules* 96, 1–10. doi: 10.1016/j.ijbiomac.2016.11.122

Roca, C., Lehmann, M., Torres, C. A. V., Baptista, S., Gaudêncio, S. P., Freitas, F., et al. (2016). Exopolysaccharide production by a marine pseudoalteromonas sp. strain isolated from Madeira archipelago ocean sediments. *New Biotechnol.* 33 (4), 460–466. doi: 10.1016/j.nbt.2016.02.005

Safaei, J., Mohamed, N. A., Noh, M. F. M., Soh, M. F., Riza, M. A., Mustakim, N. S. M., et al. (2018). Facile fabrication of graphitic carbon nitride, (g-$C_3N_4$) thin film. *J. Alloys Compd.* 769, 130–135. doi: 10.1016/j.jallcom.2018.07.337

Saravanan, C., and Shetty, P. K. H. (2016). Isolation and characterization of exopolysaccharide from *Leuconostoc lactis* KC117496 isolated from idli batter. *Int. J. Biol. Macromol.* 90, 100–106. doi: 10.1016/j.ijbiomac.2015.02.007

Satpute, S. K., Banat, I. M., Dhakephalkar, P. K., Banpurkar, A. G., and Chopade, B. A. (2010). Biosurfactants, bioemulsifiers and exopolysaccharides from marine microorganisms. *Biotechnol. Adv.* 28 (4), 436–450. doi: 10.1016/j.biotechadv.2010.02.006

Shankar, T., Palpperumal, S., Kathiresan, D., Sankaralingam, S., Balachandran, C., Baskar, K., et al. (2021). Biomedical and therapeutic potential of exopolysaccharides by lactobacillus paracasei isolated from sauerkraut: Screening and characterization. *Saudi J. Biol. Sci.* 28 (5), 2943–2950. doi: 10.1016/j.sjbs.2021.02.030

Shu, C. H., and Lung, M. Y. (2004). Effect of pH on the production and molecular weight distribution of exopolysaccharide by *Antrodia camphorata* in batch cultures. *Process Biochem.* 39 (8), 931–937. doi: 10.1016/S0032-9592(03)00220-6

Venkatesh, P., Balraj, M., Ayyanna, R., Ankaiah, D., and Arul, V. (2016). Physicochemical and biosorption properties of novel exopolysaccharide produced by *Enterococcus faecalis*. LWT-food sci. *Technol* 68, 606–614. doi: 10.1016/j.lwt.2016.01.005

Vidhyalakshmi, R., Nachiyar, C. V., Kumar, G. N., Sunkar, S., and Badsha, I. (2018). Production, characterization and emulsifying property of exopolysaccharide produced by marine isolate of *Pseudomonas fluorescens*. *Biocatalysis Agric. Biotechnol.* 16, 320–325. doi: 10.1016/j.bcab.2018.08.023

Vinothkanna, A., Sathiyanarayanan, G., Balaji, P., Mathivanan, K., Pugazhendhi, A., Ma, Y., et al. (2021). Structural characterization, functional and biological activities of an exopolysaccharide produced by probiotic *Bacillus licheniformis* AG-06 from Indian polyherbal fermented traditional medicine. *Int. J. Biol. Macromolecules* 174, 144–152. doi: 10.1016/j.ijbiomac.2021.01.117

Wagh, V. S., Said, M. S., Bennale, J. S., and Dastager, S. G. (2022). Isolation and structural characterization of exopolysaccharide from marine bacillus sp. and its optimization by microbioreactor. *Carbohydr. Polymers* 285, 119241. doi: 10.1016/j.carbpol.2022.119241

Wang, H. H., Ding, S. J., Wang, G. Y., Xu, X. L., and Zhou, G. H. (2013). *In situ* characterization and analysis of *Salmonella* biofilm formation under meat processing environments using a combined microscopic and spectroscopic approach. *Int. J. Food Microbiol.* 167 (3), 293–302. doi: 10.1016/j.ijfoodmicro.2013.10.005

Wang, Y. ,. Q., Huang, J. X., and Zhou, W. W. (2020). Isolation, characterization and cytoprotective effects against UV radiation of exopolysaccharide produced from *Paenibacillus polymyxa* PYQ1. *J. Bioscience Bioeng.* 130 (3), 283–289. doi: 10.1016/j.jbiosc.2020.05.001

Wang, Y. P., Li, C., Liu, P., Ahmed, Z., Xiao, P., and Bai, X. J. (2010). Physical characterization of exopolysaccharide produced by *Lactobacillus plantarum* KF5 isolated from Tibet kefir. *Carbohydr. Polym.* 82, 895–903. doi: 10.1016/j.carbpol.2010.06.013

Wang, J., Salem, D. R., and Sani, R. K. (2019). Extremophilic exopolysaccharides: A review and new perspectives on engineering strategies and applications. *Carbohydr. Polymers* 205, 8–26. doi: 10.1016/j.carbpol.2018.10.011

Wei, M. S., Geng, L. H., Wang, Q. C., Yue, Y., Wang, J., Wu, N., et al. (2021). Purification, characterization and immunostimulatory activity of a novel exopolysaccharide from bacillus sp. H5. *Int. J. Biol. Macromolecules* 189, 649–656. doi: 10.1016/j.ijbiomac.2021.08.159

Wiercigroch, E., Szafraniec, E., Czamara, K., Pacia, M. Z., Majzner, K., Kochan, K., et al. (2017). Raman and infrared spectroscopy of carbohydrates: A review. spectrochimica acta part a. *Mol. Biomolecular Spectrosc.* 185, 317–335. doi: 10.1016/j.saa.2017.05.045

Xu, Z. X., Chen, G. Q., Xue, L., Zhang, H. B., Wang, J. M., Xiang, H. Y., et al. (2019). Isolation, structural characterizations and bioactivities of exopolysaccharides produced by *Bacillus licheniformis*. *Int. J. Biol. Macromolecules.* 141, 298–306. doi: 10.1016/j.ijbiomac.2019.08.217

Xu, R. H., Shang, N., and Li, P. L. (2011). *In vitro* and *in vivo* antioxidant activity of exopolysaccharide fractions from *Bifidobacterium animalis* RH. *Anaerobe* 17 (5), 226–231. doi: 10.1016/j.anaerobe.2011.07.010

Yang, X. M., Wu, J. R., An, F. Y., Xu, J. W., Bat-Ochir, M., Wei, L. L., et al. (2022). Structure characterization, antioxidant and emulsifying capacities of

exopolysaccharide derived from *Tetragenococcus halophilus* SNTH-8. *Int. J. Biol. Macromolecules* 208, 288–298. doi: 10.1016/j.ijbiomac.2022.02.186

Yuan, Y. Q., Li, C., Zheng, Q. W., Wu, J. X., Zhu, K. X., Shen, X. R., et al. (2019). Effect of simulated gastrointestinal digestion *in vitro* on the antioxidant activity, molecular weight and microstructure of polysaccharides from a tropical sea cucumber (*Holothuria leucospilota*). *Food Hydrocolloid* 89, 735–741. doi: 10.1016/j.foodhyd.2018.11.040

Zhang, M., Zeng, S. Y., Hao, L. Y., Yao, S. J., Wang, D. K., Yang, H., et al. (2022). Structural characterization and bioactivity of novel exopolysaccharides produced by *Tetragenococcus halophilus*. *Food Res. Int.* 155, 111083. doi: 10.1016/j.foodres.2022.111083

Zhao, W., Zhang, J., Jiang, Y. Y., Zhao, X., Hao, X. N., Li, L., et al. (2018). Characterization and antioxidant activity of the exopolysaccharide produced by *Bacillus amyloliquefaciens* GSBa-1. *J. Microbiol. Biotechnol.* 28 (8), 1282–1292. doi: 10.4014/jmb.1801.01012